The Astrophysical Journal, 820:58 (8pp), 2016 March 20 doi:10.3847/0004-637X/820/1/58


# THE PHOENIX STREAM: A COLD STREAM IN THE SOUTHERN HEMISPHERE

E. Balbinot[1], B. Yanny[2], T. S. Li[3], B. Santiago[4,5], J. L. Marshall[3], D. A. Finley[2], A. Pieres[4,5], T. M. C. Abbott[6], F. B. Abdalla[7], S. Allam[2], A. Benoit-Lévy[7], G. M. Bernstein[8], E. Bertin[9,10], D. Brooks[7], D. L. Burke[11,12], A. Carnero Rosell[5,13], M. Carrasco Kind[14,15], J. Carretero[16,17], C. E. Cunha[11], L. N. da Costa[5,13], D. L. DePoy[3], S. Desai[18,19], H. T. Diehl[2], P. Doel[7], J. Estrada[2], B. Flaugher[2], J. Frieman[2,20], D. W. Gerdes[21], D. Gruen[22,23], R. A. Gruendl[14,15], K. Honscheid[24,25], D. J. James[6], K. Kuehn[26], N. Kuropatkin[2], O. Lahav[7], M. March[8], P. Martini[24,27], R. Miquel[17,28], R. C. Nichol[29], R. Ogando[5,13], A. K. Romer[30], E. Sanchez[31], M. Schubnell[21], I. Sevilla-Noarbe[14,31], R. C. Smith[6], M. Soares-Santos[2], F. Sobreira[2,5], E. Suchyta[24,25], G. Tarle[21], D. Thomas[29], D. Tucker[2], and A. R. Walker[6]
(The DES Collaboration)
[1] Department of Physics, University of Surrey, Guildford GU2 7XH, UK; e.balbinot@surrey.ac.uk
[2] Fermi National Accelerator Laboratory, P.O. Box 500, Batavia, IL 60510, USA
[3] George P. and Cynthia Woods Mitchell Institute for Fundamental Physics and Astronomy, and Department of Physics and Astronomy, Texas A&M University, College Station, TX 77843, USA
[4] Instituto de Física, UFRGS, Caixa Postal 15051, Porto Alegre, RS—91501-970, Brazil
[5] Laboratório Interinstitucional de e-Astronomia—LIneA, Rua Gal. José Cristino 77, Rio de Janeiro, RJ—20921-400, Brazil
[6] Cerro Tololo Inter-American Observatory, National Optical Astronomy Observatory, Casilla 603, La Serena, Chile
[7] Department of Physics & Astronomy, University College London, Gower Street, London, WC1E 6BT, UK
[8] Department of Physics and Astronomy, University of Pennsylvania, Philadelphia, PA 19104, USA
[9] CNRS, UMR 7095, Institut d'Astrophysique de Paris, F-75014, Paris, France
[10] Sorbonne Universités, UPMC Univ Paris 06, UMR 7095, Institut d'Astrophysique de Paris, F-75014, Paris, France
[11] Kavli Institute for Particle Astrophysics & Cosmology, P.O. Box 2450, Stanford University, Stanford, CA 94305, USA
[12] SLAC National Accelerator Laboratory, Menlo Park, CA 94025, USA
[13] Observatório Nacional, Rua Gal. José Cristino 77, Rio de Janeiro, RJ—20921-400, Brazil
[14] Department of Astronomy, University of Illinois, 1002 W. Green Street, Urbana, IL 61801, USA
[15] National Center for Supercomputing Applications, 1205 West Clark Street, Urbana, IL 61801, USA
[16] Institut de Ciències de l'Espai, IEEC-CSIC, Campus UAB, Carrer de Can Magrans, s/n, E-08193 Bellaterra, Barcelona, Spain
[17] Institut de Física d'Altes Energies, Universitat Autònoma de Barcelona, E-08193 Bellaterra, Barcelona, Spain
[18] Excellence Cluster universe, Boltzmannstr. 2, D-85748 Garching, Germany
[19] Faculty of Physics, Ludwig-Maximilians University, Scheinerstr. 1, D-81679 Munich, Germany
[20] Kavli Institute for Cosmological Physics, University of Chicago, Chicago, IL 60637, USA
[21] Department of Physics, University of Michigan, Ann Arbor, MI 48109, USA
[22] Max Planck Institute for Extraterrestrial Physics, Giessenbachstrasse, D-85748 Garching, Germany
[23] Universitäts-Sternwarte, Fakultät für Physik, Ludwig-Maximilians Universität München, Scheinerstr. 1, D-81679 München, Germany
[24] Center for Cosmology and Astro-Particle Physics, The Ohio State University, Columbus, OH 43210, USA
[25] Department of Physics, The Ohio State University, Columbus, OH 43210, USA
[26] Australian Astronomical Observatory, North Ryde, NSW 2113, Australia
[27] Department of Astronomy, The Ohio State University, Columbus, OH 43210, USA
[28] Institució Catalana de Recerca i Estudis Avançats, E-08010 Barcelona, Spain
[29] Institute of Cosmology & Gravitation, University of Portsmouth, Portsmouth, PO1 3FX, UK
[30] Department of Physics and Astronomy, Pevensey Building, University of Sussex, Brighton, BN1 9QH, UK
[31] Centro de Investigaciones Energéticas, Medioambientales y Tecnológicas (CIEMAT), Madrid, Spain
*Received 2015 September 10; accepted 2016 February 5; published 2016 March 17*

## ABSTRACT

We report the discovery of a stellar stream in the Dark Energy Survey Year 1 (Y1A1) data. The discovery was made through simple color–magnitude filters and visual inspection of the Y1A1 data. We refer to this new object as the Phoenix stream, after its resident constellation. After subtraction of the background stellar population we detect a clear signal of a simple stellar population. By fitting the ridge line of the stream in color–magnitude space, we find that a stellar population with age $\tau = 11.5 \pm 0.5$ Gyr and [Fe/H] $< -1.6$, located $17.5 \pm 0.9$ kpc from the Sun, gives an adequate description of the stream stellar population. The stream is detected over an extension of $8\overset{\circ}{.}1$ (2.5 kpc) and has a width of ∼54 pc assuming a Gaussian profile, indicating that a globular cluster (GC) is a probable progenitor. There is no known GC within 5 kpc that is compatible with being the progenitor of the stream, assuming that the stream traces its orbit. We examined overdensities (ODs) along the stream, however, no obvious counterpart-bound stellar system is visible in the coadded images. We also find ODs along the stream that appear to be symmetrically distributed—consistent with the epicyclic OD scenario for the formation of cold streams—as well as a misalignment between the northern and southern part of stream. Despite the close proximity we find no evidence that this stream and the halo cluster NGC 1261 have a common accretion origin linked to the recently found EriPhe OD.

*Key words:* Galaxy: halo – Galaxy: structure

## 1. INTRODUCTION

Our understanding of the structure of the Galactic halo has evolved considerably in the past two decades, largely thanks to deep and homogeneous photometric surveys, such as the Two Micron All Sky Survey (Skrutskie et al. 2006) and the Sloan Digital Sky Survey (SDSS; Ahn et al. 2014). The stellar halo is

now known to be inhabited by a variety of spatial and kinematic stellar substructure, from globular clusters (GCs) and dwarf galaxies to extended stellar clouds and streams (see, e.g., Willman et al. 2005; Belokurov et al. 2006, 2007). In fact, recent simulations based on hierarchical models of structure formation predict that most halo stars were brought by the disruption of the Galactic substructures (Bullock et al. 2001).

The thin and cold stellar streams found in the Galaxy often span tens of degrees on the sky and originate from the tidal effects of the host on the progenitor, whether a GC or a dwarf galaxy. Perhaps the most conspicuous examples of Galactic streams are those associated with the Pal 5 GC and the Sagittarius dwarf (Odenkirchen et al. 2001; Newberg et al. 2002). The tidal nature of such streams makes them useful probes of the dark matter distribution across the halo (Johnston et al. 2005; Küpper et al. 2015). Detailed modeling of a stream's position, distance, kinematics, gaps, and overdensities (ODs) in extended cold streams also leads to constraints on the amount of dark matter fragments orbiting the halo, known as subhalos (Yoon et al. 2011; Ngan et al. 2015), on the progenitor's properties and on Galactic parameters (Koposov et al. 2010).

The Dark Energy Survey (DES; The Dark Energy Survey Collaboration 2005) is an ongoing deep ($g \sim 24.7$) photometric survey in the southern hemisphere that started its planned 5-year mission of collecting data in 2013. Despite the mission's focus on cosmology, DES data have already produced a wealth of results pertaining to resolved stellar populations in the Galaxy and its vicinity, including the analysis of the structure and stellar populations in the outskirts of the Large Magellanic Cloud (LMC; Balbinot et al. 2015), the identification of new Galactic companions (Bechtol et al. 2015; Drlica-Wagner et al. 2015; Kim & Jerjen 2015; Koposov et al. 2015; Luque et al. 2016), and the development of a new search for variable stars exclusively based on DES data (D. Hatt et al. 2016, in preparation).

Here we report on the discovery of the first cold stellar stream using DES data. In Section 2 we give more details about DES, the data used, and the search algorithm. Our results are presented in Section 3 and our conclusions are in Section 4.

## 2. DATA ANALYSIS

DES is a wide-field optical imaging survey using broad photometric bands (*grizY*) performed with the Dark Energy Camera (DECam; described in detail in Flaugher et al. 2015). The DECam focal plane is comprised of 74 CCDs: 62 2k × 4k CCDs dedicated to science imaging and 12 2k × 2k CCDs for guiding, focus, and alignment. DECam is installed at the prime focus of the 4 m Blanco telescope at the Cerro Tololo Inter-American Observatory. In this configuration, DECam has a $2\overset{\circ}{.}2$ wide field-of-view and a central pixel scale of 0.263 arcseconds. The full DES survey is scheduled for 525 nights distributed over five years. Here, we consider data from the first year of DES obtained between 2013 August 15 and 2014 February 9.

The first internal annual release of DES data (Y1A1) comprises the data products obtained from the processing of a subset of wide-field and supernova-field data accumulated during the first year of DES operations (Diehl et al. 2014). Briefly, the image processing pipeline consists of image detrending (crosstalk correction, bias subtraction, flat-fielding, etc.), astrometric calibration, nightly photometric calibration, global calibration, image coaddition, and object catalog creation. For a more detailed description of the DESDM image processing pipeline, we refer to Desai et al. (2012) and Mohr et al. (2012), and for a recent overview, Balbinot et al. (2015). The SExtractor toolkit is used to create image catalogs from the processed and coadded images (Bertin 2011; Bertin & Arnouts 1996). The number of overlapping exposures in Y1A1 varies, but most of the footprint has at least three coadded exposures. The Y1A1 coadd object catalog contains ∼131 million unique objects spread over $\sim 1800\,\mathrm{deg}^2$. This area includes $\sim 200\,\mathrm{deg}^2$ overlapping with the Stripe-82 region of SDSS, as well as a contiguous region of $\sim 1600\,\mathrm{deg}^2$ overlapping with the South Pole Telescope footprint.

We perform stellar selection on the Y1A1 coadd object catalog based on the *spread_model* quantity output of SExtractor (Desai et al. 2012). To avoid issues arising from fitting the PSF across variable depth coadded images, we utilize the weighted-average (wavg) of the *spread_model* measurements from the single-epoch exposures. Our stellar sample consists of well-measured objects with $|wavg\_spread\_model\_i| < 0.003$, $flags_{\{g,r,i\}} < 4$, and $magerr\_auto\_\{g, r, i\} < 1$ (henceforth referred to as "stars"). Our stellar completeness is >90% down to magnitude $g \sim 22$, at which point it drops to ∼50% by $g \sim 23$ (Bechtol et al. 2015).

Stars are extinction-corrected according to Schlegel et al. (1998), with the scaling correction from Schlafly & Finkbeiner (2011), assuming the extinction curve from Cardelli et al. (1989) and a calibration at infinity, that is, we assume that the light of every object in our sample crosses the full extent of the dust column measured in the dust maps.

From this point all magnitudes considered in this paper are corrected for the extinction.

### 2.1. Search Method

Using the objects classified as stars according to the criteria described in the previous section, we apply narrow color filters to isolate interesting stellar types such as old turnoff stars and horizontal branch (HB) stars. To avoid issues related to the inhomogeneous photometric depth of the survey and saturation of bright stars, we only use stars with magnitudes $17 < g < 23$. We find that this magnitude limit yields a sample that has a completeness that is fairly constant across the footprint and produces a smoothly varying density for the field stars.

For each color-selected catalog we build a sky "density map." Throughout this paper we use density maps to refer to maps where we show the number of sources per pixel ($N$) in a Cartesian projection. The pixel size is made explicit whenever necessary. The pixel area is corrected for changes in solid angle with declination. These density maps are visually inspected for ODs. In Figure 1 we show the particularly interesting density map for stars with $0.2 < (g - r) < 0.6$ and $20 < g < 23$, which mainly selects turnoff and upper main-sequence stars from an old (>10 Gyr) simple stellar population (SSP), according to Bressan et al. (2012). Several features are noticeable, such as the GC NGC 1261, the Phoenix dwarf galaxy (Canterna & Flower 1977), and two of the recently discovered dwarf galaxies (Bechtol et al. 2015; Koposov et al. 2015): Reticulum II (Ret II) and Eridanus II (Eri II). These objects are labeled with their names in the figure. A linear structure is also visible near the Phoenix dwarf extending from $(\alpha, \delta) \simeq (20°, -57°)$ to $(27°, -45°)$. This structure is

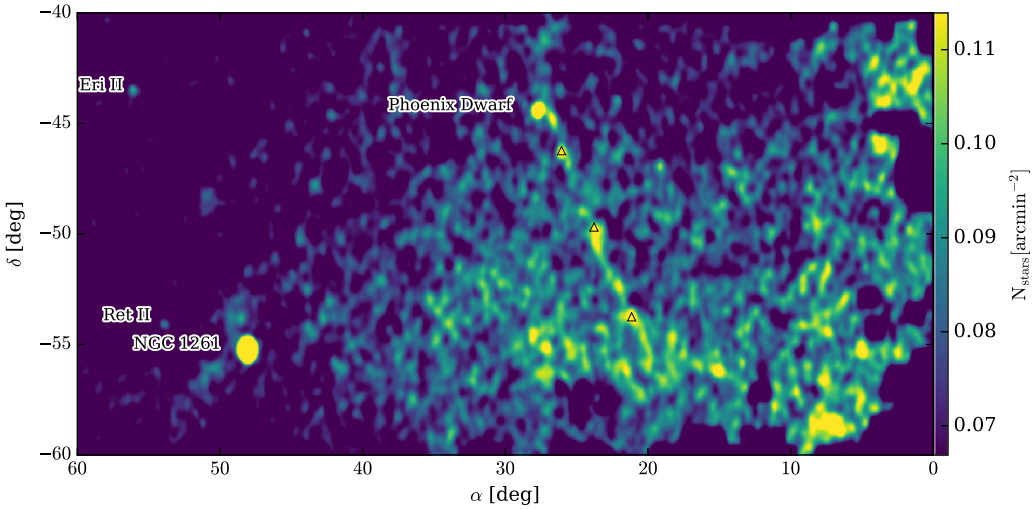


**Figure 1.** Y1A1 density map for stars with $0.2 < (g - r) < 0.6$ and $20 < g < 23$. The open triangles show the anchor points adopted for the stream. Other interesting objects are labeled in the figure. This density map was convolved with a $2 \times 1$ pixel Gaussian. Each pixel has a size of $4\farcm5 \times 2\farcm8$.

highlighted by open triangles marking high density points along the stream candidate.

In the same figure, a large OD of stars is visible between the stream candidate and NGC 1261. This feature is the Eridanus–Phoenix (EriPhe) OD and it is discussed in detail in a simultaneous publication (Li et al. 2016).

## 3. RESULTS

By means of the method outlined in the previous section we perform a visual search for stellar ODs. This search, conducted over the full Y1A1 footprint, has revealed only one[32] stream candidate, which is shown in Figure 1. For simplicity, we refer to this candidate stream as the Phoenix stream due to its proximity to the Phoenix constellation.

To study the stellar population that comprises the Phoenix stream we define a line passing through the center of the stream using anchor points along the stream (three open triangles in Figure 1). We then select stars inside a box defined by the stream central line with an offset of $\pm 0\fdg8$ in R.A. We name this selection *on stream*. To compare with the typical Milky Way (MW) stellar population at this position in the sky we select stars in boxes that are offset by $\pm 1\fdg5$ with respect to the central one and have the same width as the *on stream* region. We name these selections *off stream east* and *west*. For each region described above we compute the solid angle normalized Hess diagram. We use Mangle masks (Swanson et al. 2008) to compute the solid angle of each box, taking into account possible holes in the survey footprint. In Figure 2 we show the Hess diagram of the *on stream* minus the average diagram of the two *off stream* ones in logarithmic scale.

From the decontaminated Hess diagram shown in Figure 2 we estimate that the stream has ~500 stars that fall within the photometric limits of DES. This decontaminated Hess diagram was smoothed using a Gaussian kernel with a dispersion of $0.06 \times 0.2$ in color and magnitude, respectively. This step is required due to the low number of stars in the stream and allows us to define the ridge line shown as the red circles in Figure 2. The ridge line is defined as the peak value of counts in color for each magnitude bin, the bin size for the ridge line construction being twice as large as the one used for the Hess diagram. Magnitude bins with low counts or peak values that obviously depart from the bulk of the stream stars are

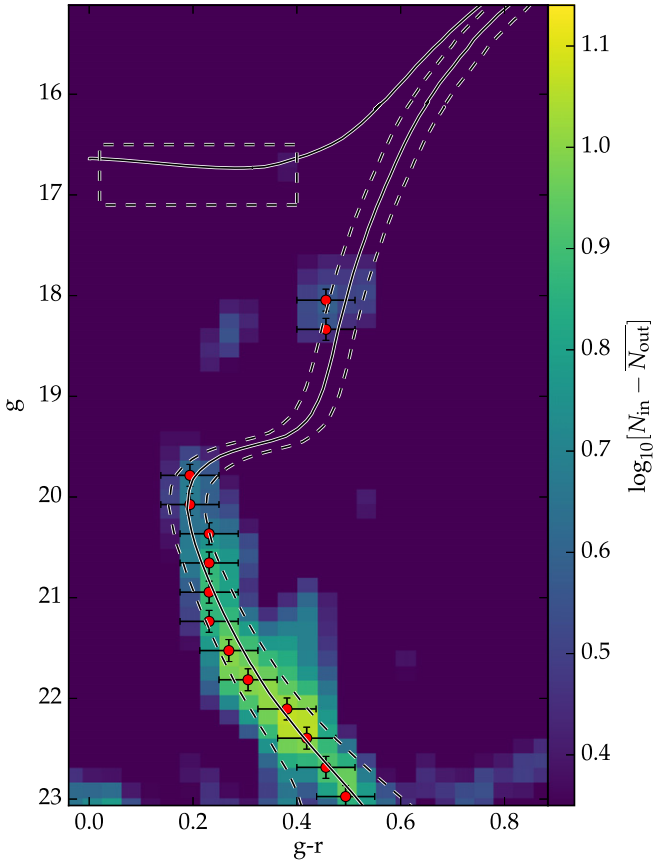


**Figure 2.** Decontaminated Hess diagram of the stream candidate. The decontamination process is described in detail in the text. The solid line shows an 11.5 Gyr and [Fe/H] = −1.9 PARSEC isochrone (Bressan et al. 2012). The dashed lines show the color–magnitude diagram (CMD) region selected to isolate stream stars, including a box to select horizontal branch (HB) stars. The red dots with error bars form the ridge line used to perform the isochrone fit.

[32] Recently Mackey et al. (2015) reported a 10 kpc-long stream associated with the LMC using a similar data set as the one in this work. We confirm this detection, however, its tidal origin is still uncertain.

**Table 1**
Phoenix Stream Parameter Summary

| Name | Value | Unit | Description |
|---|---|---|---|
| $\tau$ | $11.5 \pm 0.5$ | Gyr | Age |
| [Fe/H] | $<-1.6$ | dex | Metallicity |
| $d_{\odot}$ | $17.5 \pm 0.9$ | kpc | Heliocentric distance |
| $d_{\rm GC}$ | $18.4 \pm 0.9$ | kpc | Galactocentric distance[a] |
| $\sigma$ | 54 | pc | Stream width[b] |
| $(\alpha, \delta)_{\rm start}$ | (20, −57) | deg | Stream begin point |
| $(\alpha, \delta)_{\rm end}$ | (27, −45) | deg | Stream end point |
| $\Theta$ | 8.1 | deg | Stream length |

**Notes.**
[a] Computed using $R_{\odot} = 8.3$ kpc.
[b] Assuming a Gaussian profile.

discarded. We define the error bars as equal to the Gaussian kernel size, which is always larger than the photometric errors in the magnitude range shown. This choice of error bar accounts for the broadening of the Hess diagram due to the smoothing process. Using the typical photometric error would yield unrealistically small uncertainty estimates that would propagate into the stellar evolution model fitting, described below.

We compare the ridge line to different PARSEC stellar evolution models (Bressan et al. 2012) by computing the minimum distance from each ridge line point to a given model. The model grid has a resolution of 0.01 in $\log_{10}(\tau/\text{year})$ in the range from 9 to 10.16 and 0.0002 in $Z$ in the range from 0.0001 to 0.001, where $\tau$ and $Z$ are age and metallicity. The distance modulus was explored in the range from 15 to 18 in steps of 0.01. For each parameter combination we compute the probability that a given ridge line point was drawn from the isochrone at its minimum distance position to that given point. The probability is computed assuming a normal distribution with a $1\sigma$ dispersion as indicated by the error bars. All ridge line points are given the same weight. An obvious improvement would be to weight these points by a mass function (MF). However, the MF of a stream is likely very different from an initial MF and can vary along the stream itself (Koch et al. 2004). For this reason, we leave the study of the MF of the stream to future works with deeper photometry and more accurate membership probabilities.

We calculate a likelihood function for our model by multiplying the individual probabilities of each ridge line point. We define the best model as the one maximizing the likelihood and the parameters' uncertainties are derived using the profile likelihood technique (e.g., Rolke et al. 2005). To estimate the 90% confidence interval of each fitter parameter we find the value of that parameter where the log-likelihood (maximized with respect to the other parameters) decreases by 2.71/2 from its maximum value. We find that the stream population is well described by a model with $(m - M) = 16.21 \pm 0.11$ (or $d_{\odot} = 17.5 \pm 0.9$ kpc), $\log_{10}(\tau/\text{yr}) = 10.06 \pm 0.02$ (or $\tau = 11.5 \pm 0.5$ Gyr), and $Z < 0.0004$ (or [Fe/H] $< -1.6$). The best-fit model is shown in Figure 2 as the solid black line. Note that the lowest metallicity available in our model grid is still consistent with the stream color–magnitude diagram (CMD), thus we are only able to define a upper bound for the metallicity. We summarize the stream parameters in Table 1.

We use the best-fit model to define a region in the CMD where stream stars are more likely to be. This region is shown as the dashed line in Figure 2. The locus shown in the figure was defined by color-shifting the best-fit model by twice the typical color error at each magnitude value. We also consider that the color uncertainty at magnitudes brighter than $g = 21$ is constant and equal to 0.03.

In Figure 3 we show the density map for stars (left panel) built using the color selection described above but only for stars with $20 < g < 23$. The best-fit model describes the stream population in the full domain of colors and magnitudes observed; however, we find that the HB, sub-giant branch, and red giant branch are very sparsely populated. Including these stars in the CMD selection adds more noise than signal to our density maps. In the same figure, we also show the density map, using the same selection as before, but for sources classified as galaxies (center panel). On the rightmost panel we show a reddening map from Schlegel et al. (1998). In the last two panels the solid line shows the position of the stream. We notice no obvious features in the galaxy or reddening distribution that could mimic the presence of the stream.

### 3.1. Possible Progenitors

In order to investigate any possible progenitors for the new stream we assume that streams are approximate tracers of the progenitor's orbit (Bovy 2014). We also exploit the property of spherically symmetric potentials in which orbits should be confined to a plane containing the center of such a potential (Binney & Tremaine 2008). The same is approximately true for axisymmetric potentials (Johnston et al. 1996). For more complex potentials this assumption only holds close to the progenitor itself. There is evidence that the MW potential, at least in its inner parts, is well-approximated by an axisymmetric potential (see Küpper et al. 2015). The Phoenix stream lies at 18.4 kpc from the Galactic center where the MW potential should be reasonably spherical (Bell et al. 2008; Deason et al. 2011; Küpper et al. 2015). Under the assumption that the stream formed through the interaction with the MW potential only, we expect that it should be confined to a plane passing through the center of the Galaxy. When observed from the center of the MW this plane is described by a great circle.

To define such a plane we choose three anchor points along the stream. These points are defined by their Galactic coordinates and the heliocentric distance to the stream. We find the plane that contains the anchor points and the MW center. And finally we find the circle oriented the same way as the plane that intersects all anchor points. In order to intersect all three anchor points we must apply corrections to their heliocentric distances, which were so far considered all identical.

We find that a heliocentric distance gradient of ∼1 kpc is necessary for a circular orbit to intersect all three anchor points. In order to check this possible distance gradient we build two separate decontaminated Hess diagrams, following the same procedure outlined in Section 3: one using stars north of $\delta = -56°$ and the other using stars south of this same declination value. Using the ridge line of each of these new Hess diagrams we proceed with the fitting process; however, this time we keep the metallicity and age fixed at the best-fit values found previously using the full stream length. We find that the best-fit distance modulus for the north part of the stream is $16.19 \pm 0.12$, and $16.35 \pm 0.12$ in the south. This is

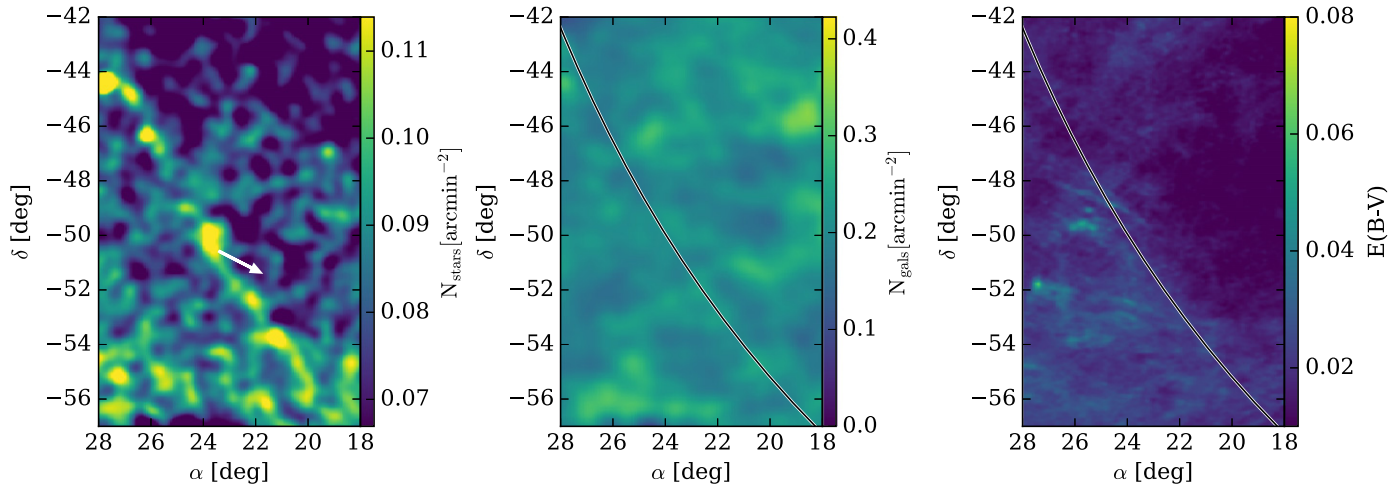


**Figure 3.** Left panel: density map after applying the color–magnitude selection shown in Figure 2. The white arrow points toward the MW center. Center panel: density map using the same filter as the previous panel but built using sources classified as galaxies. Right panel: $E(B-V)$ color excess map from Schlegel et al. (1998) and Schlafly & Finkbeiner (2011). In the last two maps the solid line shows the position of the stream as seen in the stellar density map. All maps use a pixel size of $4\farcm5 \times 2\farcm8$.

consistent with, but does not require, the ∼1 kpc gradient required for a circular orbit. We conclude that a distance gradient cannot be ruled out for the stream. Detailed spectroscopic observations must be used to isolate stream member stars based on radial velocities and chemical composition and confirm this scenario. For the purpose of looking for possible progenitors close to the stream we will assume a circular orbit.

Using the best-fit circular orbit described above, we look for possible known GCs that are not in the Y1A1 footprint that could be progenitors. This approach does not explore other kinds of orbits, which are more likely: however, it does provide a useful approach for searching for progenitors in the close vicinity of the stream. In Figure 4 we show the best-fit great circle in an all-sky Aitoff Galactic projection. We also show known GCs with galactocentric distances between 15 and 25 kpc, distances consistent with the stream distance. We find that no GC is consistent with this stream under the assumption of a circular orbit.

Another possible scenario is that the progenitor has completely dissolved and only its remains are visible along the stream. To investigate possible progenitors for this stream we first look for ODs on the stream. We start by creating a reference frame where the horizontal axis is oriented along the stream, similar to what has been adopted by Majewski et al. (2003) for the Sagittarius stream. To create such a reference frame we use two Euler angles that define two consecutive rotations ($\phi$, $\theta$). The angles were determined by finding the plane that intersects the anchor stream points in Equatorial coordinates. The new reference frame has an azimuthal component ($\Lambda$) with an arbitrary origin that is defined in the range $[0, 2\pi)$, and an elevation component ($\beta$) defined in the range $[-\frac{\pi}{2}, \frac{\pi}{2}]$. The values of $\phi$ and $\theta$ adopted are $-29\fdg698$ and $72\fdg247$, respectively.

In Figure 5 we show the density map of color-selected stars in the coordinate system described above. We also show the average density map in projection onto the $\beta$ (left panel) and $\Lambda$ (top panel) axes. The $\Lambda$ projection is shown for stars that lie within $\sigma = 0\fdg18$ from the stream centroid in $\beta$, where $\sigma$ is the standard deviation with respect to the stream median line. The stream median line is defined in the stream coordinate system

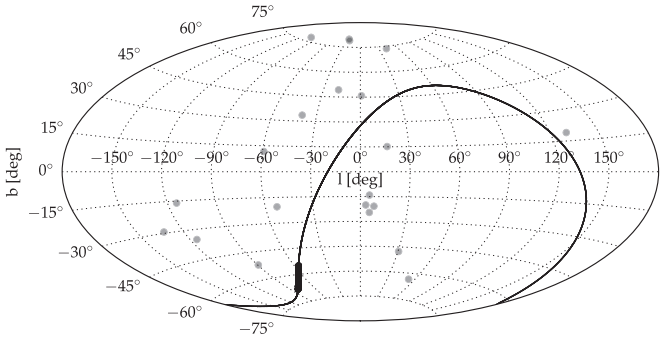


**Figure 4.** Aitoff projection in Galactic coordinates. The gray circles show GCs with galactocentric distances between 15 and 25 kpc. The solid line shows the great circle that best fits the Phoenix stream, the portion of the stream observed is highlighted with a broader line.

as the peak in the $\beta$ projected density. We also show the $\beta$ projection for stars south (green dashed line) and north (blue dashed line) of the central OD. We notice an offset of $\sim 0\fdg14$ in $\beta$ between the north and south portions of the stream.

The stream width depends on two sets of factors. The first and more obvious is the progenitor's size and velocity dispersion. The second is the shape of the gravitational potential. For instance, triaxial potentials tend to increase the fanning of stream stars significantly (Pearson et al. 2015; Price-Whelan et al. 2016). However, there is evidence that the inner halo of the Galaxy is relatively spherical (Küpper et al. 2015) out to ∼20 kpc, thus allowing us to assume the stream width maps only to the progenitor size and velocity dispersion. Using the stream coordinate system, we determine that it has an on-sky width of $\sigma = 0\fdg18$, which translates to ∼54 pc at its distance. Typically, 50 pc is consistent with the tidal radius of the MW halo GCs. The fact that the stream forms a thin coherent structure that is several kiloparsecs long makes it plausible that the progenitor was in fact a GC.

From the density projected in the $\Lambda$ coordinate we explore the presence of ODs as possible progenitors. We label these ODs in the top panel of Figure 5. First we call attention to C1 and C2, which have a slight offset with respect to each other in the $\beta$ direction, showing hints of trailing and leading tail

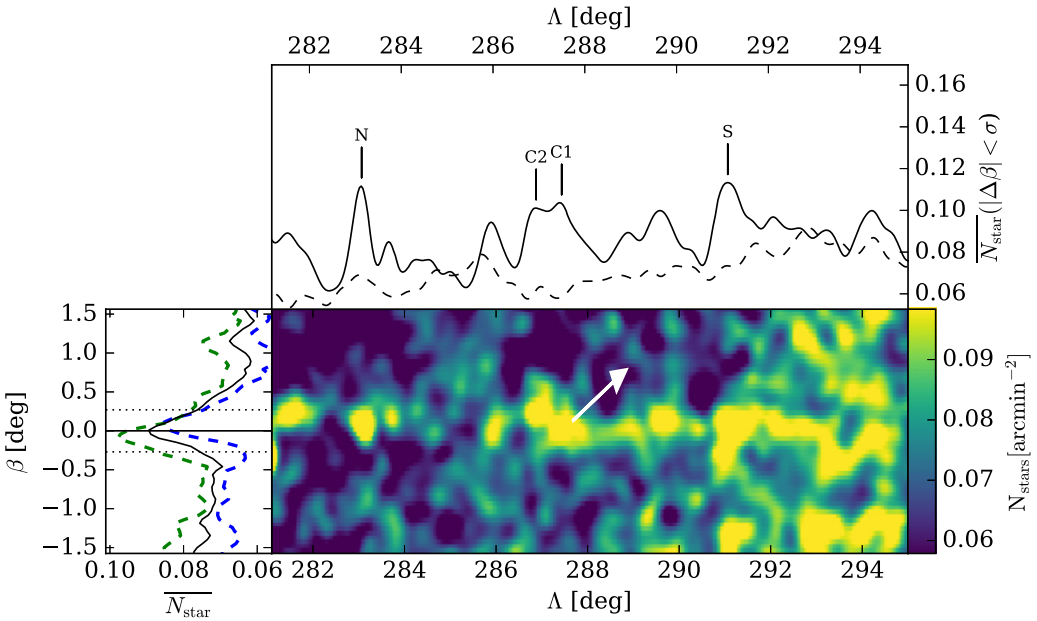


**Figure 5.** Bottom right panel: density map in the stream's coordinate system built using color–magnitude selected stars. The white arrow points toward the MW center. The pixel size is the same as in Figure 1. The dashed lines shown in Figure 2 encompass the region of the CMD from which stars were selected. The left panel shows the average density map value in projection onto the $\beta$ axis, the solid horizontal line marks the position of the stream centroid, and the dotted lines show the $\pm 1\sigma$ limits. The green (blue) dashed line shows the same kind of $\beta$ projection but for the south (north) part of the stream. The top panel shows the average density map value in projection along the $\Lambda$ axis. The latter is built using only stars that are within $\pm 1\sigma$ of the centroid of the stream. Vertical solid lines mark the position of candidate progenitors. In this panel the dashed line shows the typical background contribution, computed using stars within $\pm 1\sigma$ of a center line offset $5\sigma$ from the stream's original center line.

**Table 2**
Overdensity Positions

| OD | R.A. (deg) | Decl. (deg) | $l$ (deg) | $b$ (deg) | $\Lambda$ (deg) | $\beta$ (deg) | $\Delta\overline{\rm C1C2}$ (deg) | $\sigma$ |
|---|---|---|---|---|---|---|---|---|
| C1 | 23.75 | −49.89 | 285.68 | −65.76 | 287.50 | 0.00 | ⋯ | 5.1 |
| C2 | 23.77 | −50.40 | 286.16 | −65.28 | 286.94 | 0.22 | ⋯ | 5.0 |
| N | 26.15 | −46.34 | 277.74 | −68.10 | 283.16 | −0.09 | 4.10 | 7.1 |
| S | 21.23 | −53.70 | 292.10 | −62.72 | 291.11 | 0.03 | 4.17 | 5.0 |

misalignment with respect to the orbit (Bovy 2014). Apart from C1 and C2 we find two other peaks, one to the north (N) and another to the south (S) of the central ODs. These ODs stand out when compared to the typical background counts (dashed line in Figure 5). We compute the typical local background noise at the position of the north (south) OD by taking the standard deviation of the background counts in the north (south) portion of the stream. We find that both ODs (N & S) peak densities stand out more than $4\sigma$ with respect to the background. The significance values are listed on Table 2.

The fact that ODs N and S are approximately equally separated from the central OD could point to epicyclic ODs such as the ones reported in Küpper et al. (2015) for Palomar 5. Table 2 summarizes the positions and angular separation of the ODs with regard to the central peaks. From this table we observe that ODs to the north are systematically at higher $\beta$ than those in the south, hinting at the misalignment mentioned above.

Using the misalignment of the northern and southern portions of the stream (hinted in Figure 5), we may infer from geometrical considerations alone that its northern part is closer to the MW center, hence being formed by stars that leave the progenitor through the inner part of its orbit, forming a leading tail. By construction, the south portion forms the trailing tail. From this argument, we conclude that the stream is moving from south to north.

All ODs were visually inspected in the coadded images and catalog; however, we could not identify any stellar system (e.g., GC) that might have given origin to the stream. This result is very puzzling, especially if the scenario described above is to be confirmed. The fact that no progenitor is found, but classic signs of cold tail formation were observed, could indicate that a progenitor was fully disrupted very recently.

## 4. CONCLUSIONS

We report the discovery of a stellar stream in the southern hemisphere. Through the visual fit of stellar evolution models we find that this stream is comprised of an old ($11.5 \pm 0.5$ Gyr) metal-poor ([Fe/H] $< -1.6$) population that is 17.5 kpc away from the Sun and 18.4 kpc from the Galactic center. Though close in projection, the Phoenix stream is not related to the Phoenix galaxy, which lies 440 kpc from the Sun (Karachentsev et al. 2004).

Through the extrapolation of the stream outside the Y1A1 footprint, we found no known GC that could be its progenitor; however, more eccentric and/or non-planar orbits were not considered.

We also investigate the distribution of ODs along the stream, in search of a progenitor. We find that none of the ODs have any obvious stellar OD associated with them when coadded images were inspected. We find that the ODs with high significance display a symmetric pattern with respect to a central OD. This central OD shows some hints of misalignment perpendicular to the orbit direction, which could indicate the position of the progenitor.

A diffuse stellar OD that nearly overlaps with the Phoenix stream has recently been found in the DES data (Li et al. 2016). This OD (EriPhe) was previously hinted at by Carballo-Bello et al. (2014) as an anomalous background population close to NGC 1261. EriPhe and NGC 1261 share a similar heliocentric distance as the Phoenix stream. Using GALPY (Bovy 2015) and literature proper motions for NGC 1261 (Dambis 2006), we integrate the cluster orbit and find that it roughly aligns with the Phoenix stream and that its motion is retrograde with respect to the solar motion. The close proximity of NGC 1261 and the orbit alignment with the stream may suggest that they could share a common origin with the EriPhe OD. However, the stream appears not to be in a retrograde orbit, favoring a scenario where the stream is independent of EriPhe or NGC 1261. For an extended discussion about this scenario we refer to Li et al. (2015).

We thank Carl Grillmair for pointing out that our original derivation of the direction of motion of the stream was incorrect, and that the stream is actually moving in a prograde direction about the Galaxy.

Funding for the DES Projects has been provided by the U.S. Department of Energy, the U.S. National Science Foundation, the Ministry of Science and Education of Spain, the Science and Technology Facilities Council of the United Kingdom, the Higher Education Funding Council for England, the National Center for Supercomputing Applications at the University of Illinois at Urbana-Champaign, the Kavli Institute of Cosmological Physics at the University of Chicago, the Center for Cosmology and Astro-Particle Physics at the Ohio State University, the Mitchell Institute for Fundamental Physics and Astronomy at Texas A&M University, Financiadora de Estudos e Projetos, Fundação Carlos Chagas Filho de Amparo à Pesquisa do Estado do Rio de Janeiro, Conselho Nacional de Desenvolvimento Científico e Tecnológico and the Ministério da Ciência, Tecnologia e Inovação, the Deutsche Forschungsgemeinschaft, and the Collaborating Institutions in the Dark Energy Survey.

The Collaborating Institutions are Argonne National Laboratory, the University of California at Santa Cruz, the University of Cambridge, Centro de Investigaciones Energéticas, Medioambientales y Tecnológicas-Madrid, the University of Chicago, University College London, the DES-Brazil Consortium, the University of Edinburgh, the Eidgenössische Technische Hochschule (ETH) Zürich, Fermi National Accelerator Laboratory, the University of Illinois at Urbana-Champaign, the Institut de Ciències de l'Espai (IEEC/CSIC), the Institut de Física d'Altes Energies, Lawrence Berkeley National Laboratory, the Ludwig-Maximilians Universität München and the associated Excellence Cluster universe, the University of Michigan, the National Optical Astronomy Observatory, the University of Nottingham, The Ohio State University, the University of Pennsylvania, the University of Portsmouth, SLAC National Accelerator Laboratory, Stanford University, the University of Sussex, and Texas A&M University.

The DES data management system is supported by the National Science Foundation under grant No. AST-1138766. The DES participants from Spanish institutions are partially supported by MINECO under grants AYA2012-39559, ESP2013-48274, FPA2013-47986, and Centro de Excelencia Severo Ochoa SEV-2012-0234, some of which include ERDF funds from the European Union. Research leading to these results has received funding from the European Research Council under the European Union's Seventh Framework Programme (FP7/2007-2013), including ERC grant agreements 240672, 291329, and 306478.

This research made use of Astropy, a community-developed core Python package for Astronomy (Astropy Collaboration et al. 2013).

E. Balbinot acknowledges financial support from the European Research Council (ERC-StG-335936, CLUSTERS).

This paper has undergone internal review by the DES collaboration.

## REFERENCES

Ahn, C. P., Alexandroff, R., Allende Prieto, C., et al. 2014, ApJS, 211, 17
Astropy Collaboration, Robitaille, T. P., Tollerud, E. J., et al. 2013, A&A, 558, A33
Balbinot, E., Santiago, B. X., Girardi, L., et al. 2015, MNRAS, 449, 1129
Bechtol, K., Drlica-Wagner, A., Balbinot, E., et al. 2015, ApJ, 807, 50
Bell, E. F., Zucker, D. B., Belokurov, V., et al. 2008, ApJ, 680, 295
Belokurov, V., Zucker, D. B., Evans, N. W., et al. 2006, ApJL, 647, L111
Belokurov, V., Zucker, D. B., Evans, N. W., et al. 2007, ApJ, 654, 897
Bertin, E. 2011, in ASP Conf. Ser. 442, Astronomical Data Analysis Software and Systems XX, ed. I. N. Evans et al. (San Francisco, CA: ASP), 435
Bertin, E., & Arnouts, S. 1996, A&AS, 117, 393
Binney, J., & Tremaine, S. 2008, Galactic Dynamics (2nd ed.; Princeton, NJ: Princeton Univ. Press)
Bovy, J. 2014, ApJ, 795, 95
Bovy, J. 2015, ApJS, 216, 29
Bressan, A., Marigo, P., Girardi, L., et al. 2012, MNRAS, 427, 127
Bullock, J. S., Kravtsov, A. V., & Weinberg, D. H. 2001, ApJ, 548, 33
Canterna, R., & Flower, P. J. 1977, ApJL, 212, L57
Carballo-Bello, J. A., Sollima, A., Martínez-Delgado, D., et al. 2014, MNRAS, 445, 2971
Cardelli, J. A., Clayton, G. C., & Mathis, J. S. 1989, ApJ, 345, 245
Dambis, A. K. 2006, A&AT, 25, 185
Deason, A. J., Belokurov, V., & Evans, N. W. 2011, MNRAS, 416, 2903
Desai, S., Armstrong, R., Mohr, J. J., et al. 2012, ApJ, 757, 83
Diehl, H. T., Abbott, T. M. C., Annis, J., et al. 2014, Proc. SPIE, 9149, 0
Drlica-Wagner, A., Bechtol, K., Rykoff, E. S., et al. 2015, ApJ, 813, 109
Flaugher, B., Diehl, H. T., Honscheid, K., et al. 2015, AJ, 150, 150
Johnston, K. V., Hernquist, L., & Bolte, M. 1996, ApJ, 465, 278
Johnston, K. V., Law, D. R., & Majewski, S. R. 2005, ApJ, 619, 800
Karachentsev, I. D., Karachentseva, V. E., Huchtmeier, W. K., & Makarov, D. I. 2004, AJ, 127, 2031
Kim, D., & Jerjen, H. 2015, ApJL, 808, L39
Koch, A., Grebel, E. K., Odenkirchen, M., Martínez-Delgado, D., & Caldwell, J. A. R. 2004, AJ, 128, 2274
Koposov, S. E., Belokurov, V., Torrealba, G., & Wyn Evans, N. 2015, ApJ, 805, 130
Koposov, S. E., Rix, H.-W., & Hogg, D. W. 2010, ApJ, 712, 260
Küpper, A. H. W., Balbinot, E., Bonaca, A., et al. 2015, ApJ, 803, 80
Li, T. S., Balbinot, E., Mondrik, N., et al. 2016, ApJ, 817, 135
Luque, E., Queiroz, A., Santiago, B., et al. 2016, MNRAS, 458, 603
Mackey, D., Koposov, S. E., Erkal, D., et al. 2015, MNRAS, in press (arXiv:1508.01356)
Majewski, S. R., Skrutskie, M. F., Weinberg, M. D., & Ostheimer, J. C. 2003, ApJ, 599, 1082
Mohr, J. J., Armstrong, R., Bertin, E., et al. 2012, Proc. SPIE, 8451, 84510D
Newberg, H. J., Yanny, B., Rockosi, C., et al. 2002, ApJ, 569, 245
Ngan, W., Bozek, B., Carlberg, R. G., et al. 2015, ApJ, 803, 75
Odenkirchen, M., Grebel, E. K., Rockosi, C. M., et al. 2001, ApJL, 548, L165

Pearson, S., Küpper, A. H. W., Johnston, K. V., & Price-Whelan, A. M. 2015, ApJ, 799, 28
Price-Whelan, A. M., Johnston, K. V., Valluri, M., et al. 2016, MNRAS, 455, 1079
Rolke, W. A., López, A. M., & Conrad, J. 2005, NIMPA, 551, 493
Schlafly, E. F., & Finkbeiner, D. P. 2011, ApJ, 737, 103
Schlegel, D. J., Finkbeiner, D. P., & Davis, M. 1998, ApJ, 500, 525
Skrutskie, M. F., Cutri, R. M., Stiening, R., et al. 2006, AJ, 131, 1163
Swanson, M. E. C., Tegmark, M., Hamilton, A. J. S., & Hill, J. C. 2008, MNRAS, 387, 1391
The Dark Energy Survey Collaboration 2005, arXiv:astro-ph/0510346
Willman, B., Dalcanton, J. J., Martinez-Delgado, D., et al. 2005, ApJL, 626, L85
Yoon, J. H., Johnston, K. V., & Hogg, D. W. 2011, ApJ, 731, 58